

# Electronic and Magnetic Properties of Kremer's tris-Hydroxo Bridged Chromium Dimer: A Challenge for DFT

Simon J. Bennie,\* David Collison, and Joseph J. W. McDouall

School of Chemistry, The University of Manchester, Oxford Road, Manchester, M13 9PL, United Kingdom

**ABSTRACT:** We present computations of the zero field splitting constants in a tris-hydroxo bridged chromium dimer (Kremer's dimer). A comparison is given of broken symmetry density functional theory (DFT) and multiconfigurational *ab initio* methods for evaluating ZFS constants. Kremer's dimer is known to be antiferromagnetically coupled, with the spin ladder order of  $E(S=0) < E(S=1) < E(S=2) < E(S=3)$ . The B3LYP functional gives the order  $E(S=0) < E(S=3) < E(S=1) < E(S=2)$ , and similar results are obtained for other density functionals (PBE, M06, M06-L, and TPSS). In contrast, we find that simple CASSCF calculations yield a correct spin ladder. DFT poorly reproduces the experimental  $D$  splitting values, while the CASSCF technique coupled with quasi-degenerate perturbation theory qualitatively reproduces  $D$  for all the spin states. State-optimized orbitals result in more accurate spin state energies and  $D$  values compared to state-averaged orbitals. Inclusion of spin–spin coupling is found to be essential for both the magnitude and sign of  $D$ . The rhombic splitting parameter is found to be near zero, which is comparable to experimental results for which the analysis assumed  $C_{3h}$  symmetry.

## INTRODUCTION

Zero field splitting (ZFS) is one of the most challenging magnetic phenomena to reproduce and to predict using computational quantum chemistry. Often it manifests as energy level splittings of around  $1\text{ cm}^{-1}$  arising from the interaction of near degenerate states. The need to develop a new generation of magnetic devices to replace current magnetotopical storage has led to an increased interest in the phenomenon. Inorganic chemists in particular have focused on the construction of single molecule magnets (SMMs) for this purpose.<sup>1,2</sup> SMMs have the potential to allow magnets to be constructed using a bottom up approach to store data at a purely quantum level and may offer a high-density solution for information storage. The main issue facing this technology is that the current generation of SMMs cannot store data at useful temperatures. SMMs encode information in their spin orientation, the stability of which, for d metal compounds, depends on an energy barrier,  $\Delta E$  (eq 1).

$$\Delta E = S^2 |D| \quad (1)$$

In eq 1,  $S$  is the total spin of the system and  $|D|$  is the magnitude of the axial (or large) component of the zero field splitting (ZFS) which arises in the spin Hamiltonian

$$\hat{H}^{\text{ZFS}} = \hat{S}_z^2 - \frac{1}{3}(S(S+1))D - (\hat{S}_x^2 - \hat{S}_y^2)E \quad (2)$$

The axial ZFS splitting constant is given by

$$D = D_{zz} - \frac{1}{2}(D_{xx} + D_{yy}) \quad (3)$$

in which  $D_{xx}$ ,  $D_{yy}$ , and  $D_{zz}$  are the eigenvalues of the ZFS tensor. The  $z$  axis is taken as corresponding to the direction of largest magnitude. The  $E$  factor in eq 2 is the rhombic splitting of the microstates; it does not directly influence the energy barrier and is not as important in the construction of SMMs. Following an initial selective population of spin states by interaction with a magnetic field, the energy barrier (eq 1) prevents a return to the disordered equilibrium distribution of spin orientations.

According to eq 1, SMMs with a large barrier can be constructed by increasing the maximum spin of the system,  $S$ . Two main routes are available to increase  $S$ , either through the ferromagnetic coupling of metals, or by antiferromagnetic coupling of an odd number of metal centers, which results in an uneven spin distribution. It is also possible to employ metal centers carrying different spins, such that the overall spin cannot be quenched by spin-pairing. An alternative route to increase the energy barrier is via  $D$ ; however, it is the more subtle component and can be strongly influenced by ligand effects, such as Jahn–Teller distortions.<sup>3</sup> Changing both  $S$  and  $D$  is thus a chemical challenge, and theory can be of great use if accurate values of  $D$  can be obtained using computational techniques, especially since achieving an increase in one parameter can often result in a decrease in the other.<sup>4</sup>

ZFS arises from the interaction of the intrinsic magnetic moments of unpaired electrons and hence only occurs when  $S > 1/2$ . Each unpaired electron is able to interact with the magnetic moment of another electron causing a splitting of energy levels in the absence of an external magnetic field. Knowing the order of the magnetic sublevels, it is possible directly to extract the magnitude and sign of  $D$  and  $E$ , the rhombic splitting, using eq 2.

The ZFS arises on a first-order level due to a direct dipolar coupling between separate electrons, called spin–spin coupling (SS).<sup>5,6</sup> The anisotropy arising from the SS coupling is dependent only on the spin density and is relatively simple to calculate. The second, more complex, mechanism of interaction is the spin–orbit coupling (SOC). The total SOC for each electron is dependent on coupling of its spin with its own orbital angular momentum and also its interaction with the orbital angular momenta of the other electrons around it (spin-other-orbit interaction).<sup>7</sup> This is more challenging to calculate as the

**Special Issue:** Berny Schlegel Festschrift

**Received:** July 19, 2012



reference state is able to interact with nearby states of the same multiplicity,  $S$ , and with states that differ by  $S \pm 1$ . This is closely related to the way in which the  $g$  factor is calculated from the SOC, but it is the inclusion of the  $S \pm 1$  states that causes the additional complication and is perhaps the reason that the ZFS is, computationally, the lesser-studied phenomenon. In this work, we use a mean field spin–orbit operator for computational efficiency. The specific form of the operator we use is that described by Hess et al.<sup>8</sup> and denoted as SOMF(1X), indicating that the one-center approximation is applied to the exchange terms only, with all other components including full multicenter terms. SOMF(1X) has been shown to provide good accuracy in application to the calculation of electronic  $g$  matrices.<sup>9</sup>

We focus on three methods to calculate the ZFS from the SOC perturbation, two of them within a density functional theory (DFT) framework and one wave-function-based method. The two methods used with DFT are both due to Neese.<sup>5,10</sup> The first is an uncoupled perturbed method, in which quasi-restricted orbitals (QRO) are used to reinforce spin symmetry following spin-unrestricted calculations. The second, coupled-perturbed method (CP) was designed to allow for the inclusion of exact exchange. In ref 5, Van Wullen offers a detailed description of both methods as well as some advances in the formulation of the CP technique.

The wave function approaches we have used involve both state optimized and state averaged complete active space self-consistent field (CASSCF) calculations. Using the CASSCF states, quasi-degenerate perturbation theory (QDPT)<sup>11</sup> was used to include the SOC effects, and the ZFS was obtained directly from the microstate energy splitting.

We have previously conducted investigations into ZFS for molecules containing one metal center.<sup>12</sup> Our focus was to understand the computational parameters that are important in calculating reliable  $D$  values. We studied a range of metals with varying ZFS values and d orbital occupations (V(III), Cr(III), Mn(III), and Fe(III)). We found that generalized-gradient approximation (GGA) functionals generally outperformed hybrid functionals in reproducing  $D$  values. We also found it important to use large uncontracted basis sets on the metal centers. These strategies enabled us to calculate values of  $|D|$  to ~20% of the experimental values.

Most theoretical literature (e.g., refs 5 and 6) on ZFS currently focuses on monometallic systems. However, the interaction between metals is key to advancing the understanding of ZFS, as the experimental drive has been to molecules with multiple centers. Kremer's dimer<sup>13,14</sup> (Figure 1) is an ideal candidate for studying ZFS with two metal centers.

The dimer consists of two chromium(III) ions bridged by three  $\mu$ -OH ions, and each metal is capped by a neutral tridentate triazacyclononane ligand. The trication was crystallized as a tris iodide salt. The counterions are not considered in this work. There are six magnetically active electrons, which couple to produce four distinct spin states. The lowest energy state is the antiferromagnetic  $S = 0$  ground state, which is magnetically inactive, followed by  $S = 1$ , then the  $S = 2$  state, and the highest energy  $S = 3$  state. The energy separation between these states and their respective ZFS values has been well characterized by experimentation (Figure 2).

## COMPUTATIONAL DETAILS

In this study, the Gaussian<sup>15</sup> and ORCA<sup>16</sup> computational chemistry suites were used. All of the reported ZFS values were

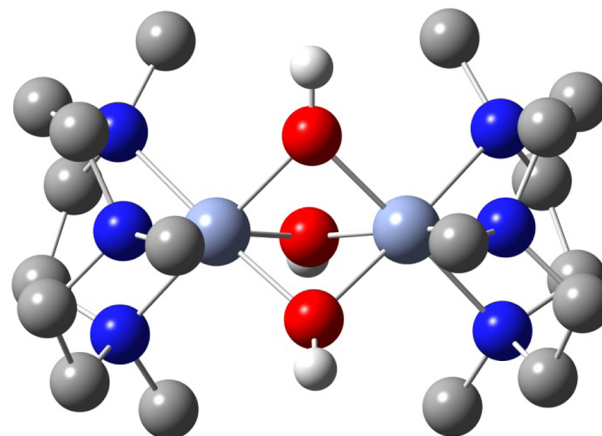


**Figure 1.** Structure of tris( $\mu$ -hydroxo)bis[(1,4,7-trimethyl-1,4,7-triazacyclononane)chromium(III)]<sup>3+</sup>. Hydrogens on terminal ligands omitted for clarity. C, gray; Cr, light blue; H, white; O, red; N, dark blue.

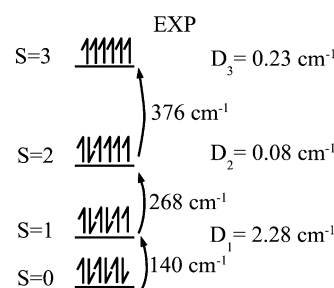


**Figure 2.** Experimentally determined energy levels and their axial ZFS values. Relative energies and  $D$  in  $\text{cm}^{-1}$ .

calculated using ORCA. We investigated the performance of unrestricted PBE,<sup>17</sup> TPSS,<sup>18</sup> B3LYP,<sup>19–22</sup> M06,<sup>23</sup> and M06-L<sup>24</sup> exchange-correlation functionals, as well as the  $D$  splitting for the TPSS, PBE, and B3LYP functionals. The DFT-based ZFS calculations included scalar relativistic corrections at the level of the zero-order regular approximation (ZORA).<sup>25–28</sup> The relative energies of the spin states obtained with the M06 functional did not include relativistic corrections. All calculations used fine grids to avoid numerical noise, with particular resolution on chromium for calculations of the ZFS. We employed the Ahlrichs Def2 basis set family.<sup>29,30</sup> For the DFT calculations, as in our previous work, we used an uncontracted quadruple- $\zeta$  basis for the metal (QZVP) and a regular contracted split valence basis for the ligands (SVP); we denote this combined basis as QZVP-SVP. For CASSCF calculations, we used the standard contracted basis sets on all atoms. The crystal structure given in ref 31 was used, with the positions of the hydroxo hydrogen atoms being optimized at the BLYP/SVP level.

## DISCUSSION

Our initial focus is the order of the spin states obtained from DFT calculations. In Figure 3, we report the energy levels using various exchange-correlation functionals. For each functional, the spin ladder was calculated starting from the converged  $S = 3$  state with subsequent pairing of high spin orbitals to produce the required spin. In each case, we confirmed the correct pairing of orbitals in the broken symmetry solutions through a visual check of the orbitals as well as inspection of the Mulliken spin densities. The Mulliken spin densities are included in Table 1. For the  $S = 1$

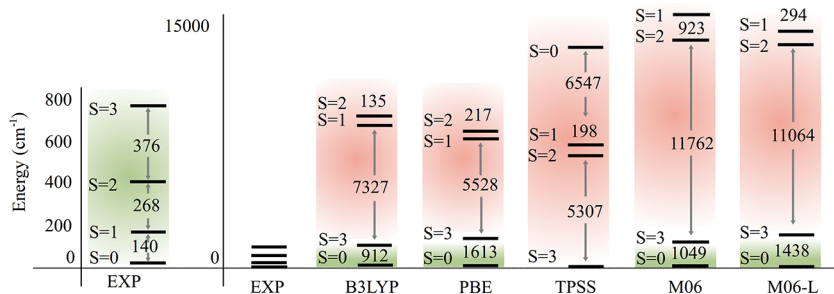


**Figure 3.** Ordering of energy levels of spin  $S = 0, 1, 2, 3$ . Experimental results are shown on an expanded scale and also on the same scale as the DFT calculations. Relative energies in  $\text{cm}^{-1}$ .

**Table 1. The Mulliken Spin Densities for the Chromium Atoms for Various DFT Functionals**

	B3LYP		PBE		TPSS		M06		M06-L	
	Cr <sub>1</sub>	Cr <sub>2</sub>								
$S = 0$	2.97	-2.97	2.90	-2.90	2.88	-2.88	3.16	-3.16	2.87	-2.87
$S = 1$	2.99	-0.94	2.90	-0.84	2.86	-0.86	3.23	-1.04	2.92	-0.85
$S = 2$	3.04	1.07	2.89	1.25	2.84	1.14	3.29	1.14	2.93	1.24
$S = 3$	3.07	3.07	3.09	3.09	3.05	3.05	3.36	3.36	3.12	3.12

state, it was found that the solution with equivalent spins on both Cr atoms was of higher energy than the solution reported in Table 1. This can be explained by considering the nature of the exchange interactions. The solution corresponding to Table 1 localizes the beta electrons to Cr<sub>2</sub> and thus increases the single center exchange interactions on Cr<sub>1</sub>, lowering the energy.

None of the functionals tested gave the correct ordering of spin states. Many calculations were attempted in which occupied and virtual orbitals were swapped and reoptimized in an attempt to ensure that a global minimum was reached for each spin multiplicity.

The TPSS functional resulted in an inverted ladder. The energy difference between the  $S = 0$  and  $S = 3$  states is  $784 \text{ cm}^{-1}$  according to experimental results. This was reproduced most closely by the B3LYP and M06 functionals, with errors of  $128 \text{ cm}^{-1}$  and  $265 \text{ cm}^{-1}$ , respectively. The PBE and M06-L functionals resulted in an energy gap that was too large by approximately a factor of 2. For all of the functionals tested, the  $S = 1$  and  $S = 2$  states were problematic and gave energies that are many thousands of wavenumbers too high. It is clear from these results that standard DFT encounters some difficulty in reproducing the spin energy ladder of Kremer's dimer.

The eigenvalues of  $\hat{S}^2$  shown in Table 2 indicate that the  $S = 0$ ,  $S = 1$ , and  $S = 2$  states are of broken spin symmetry for all

**Table 3.  $D$  Values ( $\text{cm}^{-1}$ ) Obtained with DFT and the CP or QRO Methods**

state	exptl. $ D $	B3LYP-CP	B3LYP-QRO	PBE-CP	PBE-QRO	TPSS-CP	TPSS-QRO
$S = 1$	2.20	-0.73		3.13		-3.63	
$S = 2$	0.08	14.33	0.27	1.63		1.37	0.66
$S = 3$	0.24	0.07	0.05	0.12	0.14	0.10	0.12

contamination precludes the use of the QRO method for these. The B3LYP-CP combination gives the poorest values and is the only functional to underestimate  $D$  for the  $S = 1$  state. This level also resulted in the  $D$  value of the  $S = 2$  state being wildly overestimated.

For the  $S = 1$  state, the B3LYP-CP method inverts the sign of  $D$  and gives an excessively small magnitude. Conversely, the PBE-CP and TPSS-CP methods produce values that are too large. The QRO method is not applicable to the  $S = 1$  state given the very significant spin contamination present. Similarly, all methods produced values of  $D$  for the  $S = 2$  state that were 1 to 2 orders of magnitude too large. All of the tested combinations of density functionals and CP or QRO methods resulted in  $D$  values that are too large for the  $S = 2$  state.

The  $D$  values for the  $S = 3$  state were universally too small but did approach the experimental value within a factor of 2. In this case, where the QRO method was applicable because of the small degree of spin contamination, very little difference was observed between the CP and QRO results.

The broken spin symmetry solutions obtained for Kremer's dimer suggest the presence of multiconfigurational character, through showing spin contamination of higher states. Given the poor estimates of the spin state ordering, and the values of  $D$ , it may be assumed that the degree of multiconfigurational character is sufficiently strong that the broken symmetry density functional approach cannot adequately deal with it. To investigate this suggestion, we performed complete active space self-consistent field (CASSCF) calculations. We began with the ground state ( $S = 0$ ) by finding the 10 molecular orbitals comprised of the 3d orbitals of the Cr atoms. The six lowest energies of these orbitals were included in the active space along with the six electrons coming from the metal centers. Following orbital optimization, the six orbitals shown in Figure 4 were obtained.

**Table 2. The  $\hat{S}^2$  Eigenvalues for Each Spin State with the Density Functionals Used**

state	$S(S + 1)$	B3LYP	PBE	TPSS	M06	M06-L
$S = 0$	0	2.99	2.89	2.79	3.06	2.97
$S = 1$	2	3.93	3.82	3.60	3.99	3.90
$S = 2$	6	6.96	6.72	6.63	6.96	6.79
$S = 3$	12	12.04	12.05	12.03	12.11	12.07

functionals used. The  $S = 3$  state possesses little spin contamination for any functional.

The  $D$  splittings corresponding to the states shown in Figure 3 are given in Table 3. We have omitted the QRO results for some of the exchange-correlation functionals since the degree of spin

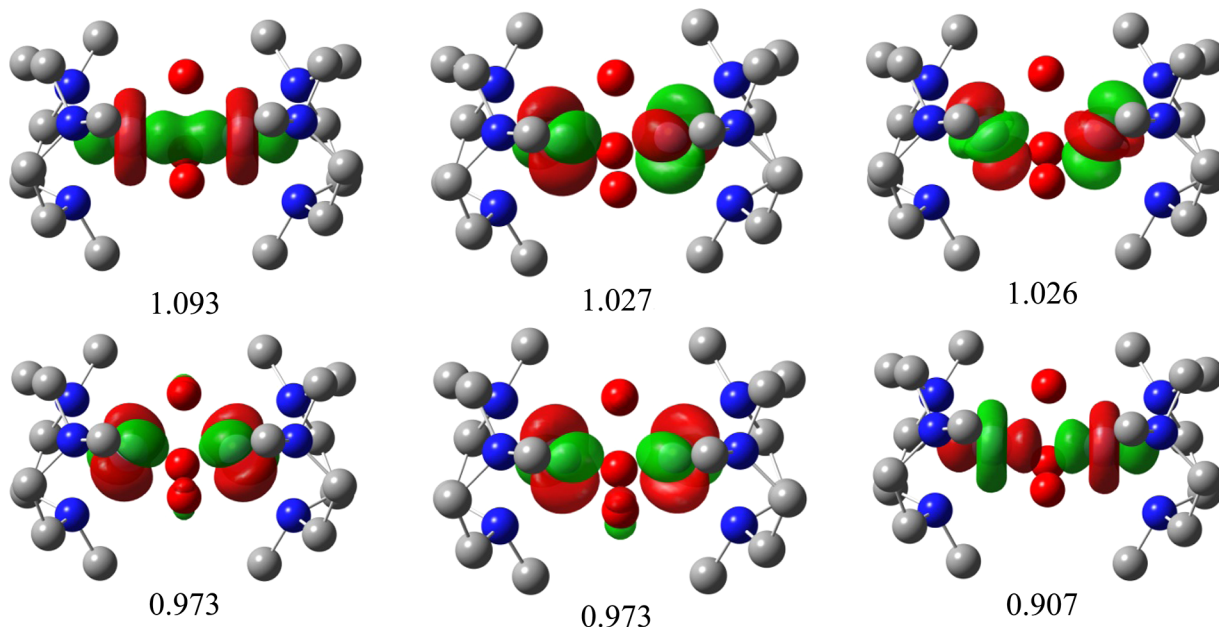


**Figure 4.** The active orbitals from the CASSCF(6,6)/SVP for the  $S = 0$  state and their natural orbital occupation numbers.

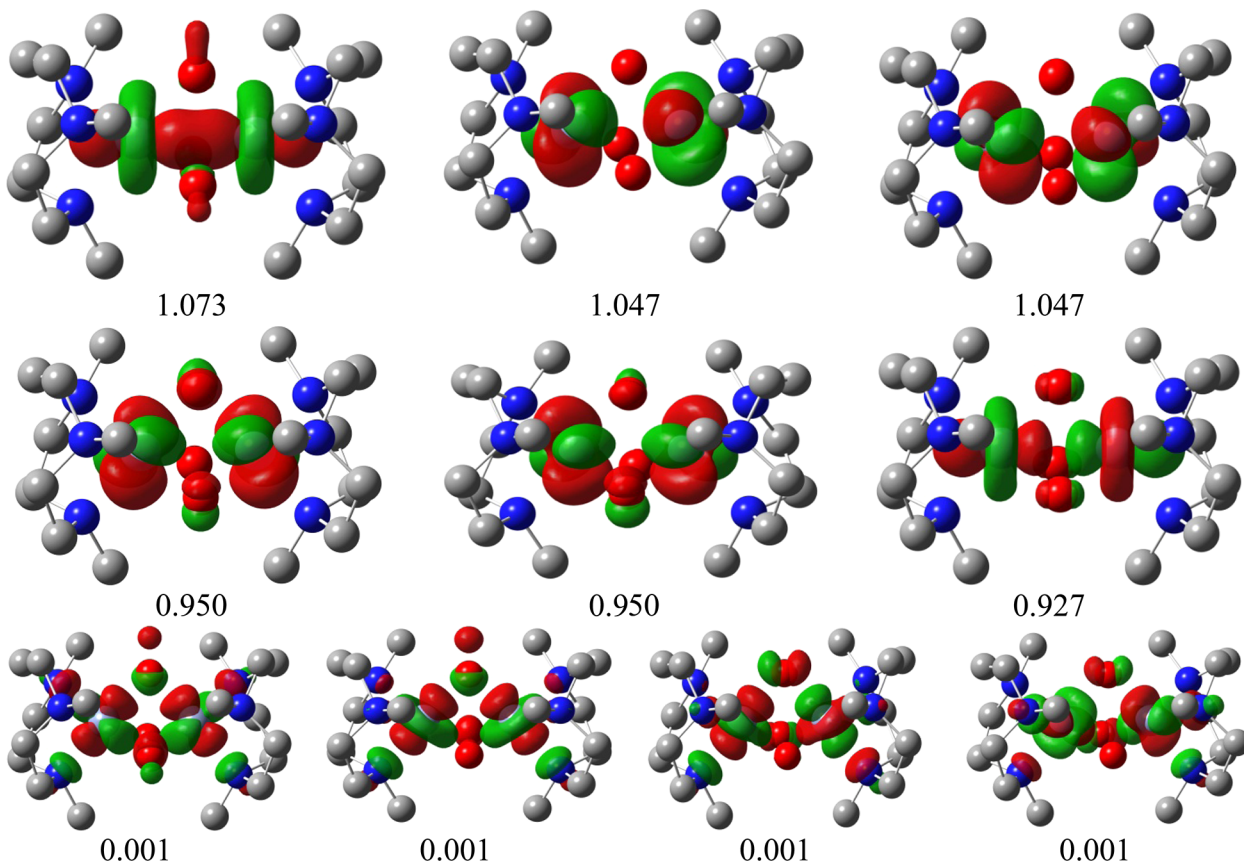


**Figure 5.** The active orbitals at the SA-CASSCF(6,10)/SVP level. The averaging is over the ground state for each spin multiplicity. Natural orbital occupation numbers are shown.

The natural orbital occupation numbers are shown alongside each orbital, and it can be seen that the  $S = 0$  state is an open-shell spin-paired state with each orbital having an occupancy of about 1. The dominant configuration state function (CSF) has a coefficient of only 0.28, with the next 20 most significant CSFs having coefficients of about 0.1. These data all indicate a strongly

multiconfigurational structure. A similar situation was found for the  $S = 1$  and  $S = 2$  states. Accordingly, we performed a number of state-optimized CASSCF and state-averaged (SA-CASSCF) calculations, including the remaining 3d orbitals, i.e., CASSCF(6,10) calculations, to characterize the spin states. Figure 5 shows the converged orbitals of the SA-CASSCF(6,10). The SA-CASSCF(6,10)

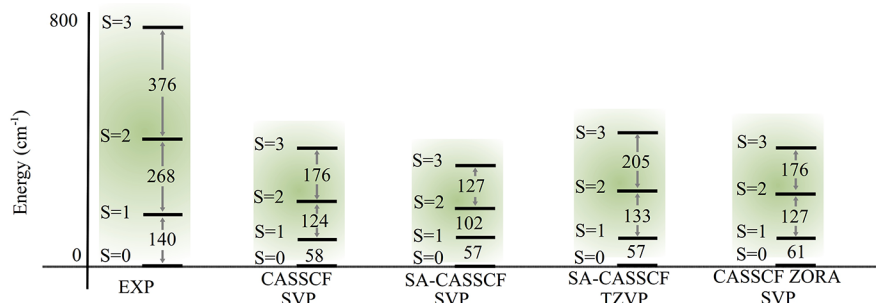


**Figure 6.** Relative ordering of energy levels from CASSCF(6,10) and SA-CASSCF(6,10) calculations, see text. Relative energies in  $\text{cm}^{-1}$ .

calculations correspond to an equal weight averaging over the lowest root of each spin multiplicity. The strongly occupied orbitals are qualitatively indistinguishable from those of the state optimized CASSCF(6,6). Figure 6 shows the ordering of energy levels obtained from CASSCF(6,10) and SA-CASSCF(6,10) calculations.

The state optimized CASSCF calculations correctly reproduce the state ordering, although the energy gaps are a factor of 2 smaller than experimental results. This is in stark contrast to the results from DFT shown in Figure 3. The SA-CASSCF calculations produce slightly smaller energy gaps. We also tried increasing the size of the basis on the Cr atoms and including ZORA corrections, but these had relatively little effect on the energy level splittings.

Turning now to the calculation of  $D$ , we used a QDPT framework to calculate the ZFS, in which states corresponding to the roots of the CASSCF method are mixed under the spin-orbit operator. All the necessary states for the ZFS are accounted for by including spin states with  $\Delta S = 0, \pm 1$  for each reference state; e.g., for the  $S = 2$  reference state,  $S = 1$ ,  $S = 2$ , and  $S = 3$  states are included in the QDPT. A large span of state energies, amounting to an interval  $>6$  eV, were allowed to mix in the spin orbit treatment. We varied the number of states of each spin multiplicity that were state-averaged. The variation in the predicted  $D$  values is shown in Table 4.

**Table 4.**  $D$  Values ( $\text{cm}^{-1}$ ) from SA-CASSCF(6,10) Calculations<sup>a</sup>

spin state	exptl. $ D $	10 states	20 states	30 states	40 states	50 states
$S = 1$	2.2	-0.653	-2.199	-1.913	-1.923	-1.767
$S = 2$	0.08	0.121	0.138	-0.097	-0.029	-0.048
$S = 3$	0.24	-0.006	0.413	0.166	0.092	0.142

<sup>a</sup>The number of states specified refers to the number taken from each of the  $S = 0, 1, 2, 3$  states.

We cannot expect monotonic convergence for this process with respect to the number of roots included in the state averaging, because the inclusion of increasing numbers of higher lying states will degrade the description of the lower lying electronic states. From the results in Table 4, we find a reasonable stability of the results with the inclusion of 40–50 states from each spin multiplicity. The best results compare well with the small splitting from experimental results for the  $S = 2$  state and the large splitting of the  $S = 1$  state.

We also investigated the effect on the results from varying the different spin states included in the state-averaging process. Table 5 shows  $D$  to be relatively insensitive to the spin states that are included in the state-averaging. The results of the [0,1,2,3] set (second column) are the same as the 50 state selection in Table 3.

**Table 5.**  $D$  Values ( $\text{cm}^{-1}$ ) Obtained with the Inclusion of Different Spin Multiplicities in the State-Averaging Process<sup>a</sup>

spin state	exptl. $ D $	[0,1,2,3]	[0,1,2]	[1,2,3]	[2,3]
$S = 1$	2.2	-1.767	-1.767	-1.943	
$S = 2$	0.08	-0.048	-0.035	0.016	-0.143
$S = 3$	0.24	0.142		0.155	0.173

<sup>a</sup>All calculations refer to SA-CASSCF(6,10). Given in square brackets are the spin states included.

The  $D$  splittings closest to experimental results are obtained when using orbitals averaged without the  $S = 0$  state. In particular, the [1,2,3] configuration gives results reasonably comparable to experimental results. The removal of the  $S = 0$  state should be unimportant to the ZFS values, as it is magnetically inactive. Removal of the  $S = 0$  states changes the sign of  $D$  in the  $S = 2$  state, showing the importance of choosing an appropriate set of spin states in the state-averaging process.

Finally, the ZFS values were calculated with orbitals optimized for each reference (ground state) spin multiplicity, see Table 6.

**Table 6.**  $D$  Values ( $\text{cm}^{-1}$ ) Obtained with State Optimized Orbitals<sup>a</sup>

state optimized	exptl. $ D $	$D (S = 1)$	$D (S = 2)$	$D (S = 3)$
$S = 1$	2.2	<b>-2.608</b>	-2.008	not included
$S = 2$	0.08	0.044	<b>0.027</b>	-0.141
$S = 3$	0.24	not included	0.175	<b>0.187</b>

<sup>a</sup>Bold values on the diagonal shown are the  $D$  values from orbitals optimized for that spin state.

The  $S = 1$  optimized orbitals resulted in a  $D$  value that is too large; this was not observed in any of the other CASSCF calculations. For the  $S = 2$  state,  $D$  is  $0.019 \text{ cm}^{-1}$  away from experimental results when calculated with  $S = 2$  orbitals and is among the best values for this state that we have obtained. For the  $S = 3$  state,  $D$  differs from experimental results by just  $0.053 \text{ cm}^{-1}$ . An interesting trend can be found when comparing this result to the state averaged values from Table 4. There is an improvement in agreement with experimental results of the  $D$  splitting upon removal of the averaging of other states; i.e., removal of the  $S = 0$  state increases the splitting by  $0.012 \text{ cm}^{-1}$ . The additional removal of the  $S = 1$  state further improves the value by another  $0.019 \text{ cm}^{-1}$ , and using state optimized ( $S = 3$ ) orbitals yields a further improvement of  $0.014 \text{ cm}^{-1}$ . This can be traced to the fact that the  $S = 3$  is the highest lying state and has a large energy gap with the  $S = 2$  state; it appears that the character of the other states may be causing degradation of  $D$  for the  $S = 3$  state.

An advantage that theoretical chemistry has to offer experimentation is the ability to extract the components of the ZFS and provide an analysis that can aid in the design of SMMs. Using the SA-CASSCF results that we have described, we illustrate that the SS contribution to  $D$  for this molecule is not insignificant, see Table 7. The  $S = 1$  state shows a large

**Table 7. The Breakdown of the Spin–Spin and Spin–Orbit Components for the SA-CASSCF [0,1,2,3]**

spin state	exptl. $ D $	spin–spin $\text{cm}^{-1}$	spin–orbit $\text{cm}^{-1}$	total $\text{cm}^{-1}$
$S = 1$	2.2	-0.673	-1.091	-1.767
$S = 2$	0.08	-0.107	0.063	-0.048
$S = 3$	0.24	-0.015	0.159	0.142

contribution,  $-0.67 \text{ cm}^{-1}$ , which adds to the SOC component. The  $S = 2$  and  $S = 3$  states have negative SS components which act to reduce the overall effect of the SOC term. In particular, the SS contribution for the  $S = 2$  state is larger than the SOC contribution. In our earlier discussion, we mentioned that the  $S = 2$  state optimized orbitals have a different sign for  $D$  than for the state averaged set (Table 6); this can be traced to an increase in the SOC term, which goes from  $0.063 \text{ cm}^{-1}$  to  $0.150 \text{ cm}^{-1}$  upon using state optimized orbitals. The degree of this contribution is significant and shows that its inclusion is necessary in any future calculation of ZFS values.

The rhombic splitting parameter ( $E$ ), being half the splitting between the  $M_s = \pm 1$  microstates, was also calculated. Kremer's<sup>14</sup> analysis assumes  $C_{3h}$  symmetry to derive the  $D$  values.  $C_{3h}$  implies axial symmetry and  $E = 0$ .

$E$  was less than  $0.03 \text{ cm}^{-1}$  for all of the states and methods utilized. The state-optimized orbitals in Table 8 have much larger

**Table 8.  $E$  Values ( $\text{cm}^{-1}$ ) Obtained with State Optimized Orbitals<sup>a</sup>**

state optimized	$E$ ( $S = 1$ )	$E$ ( $S = 2$ )	$E$ ( $S = 3$ )
$S = 1$	<b>0.029</b>	0.027	
$S = 2$	0.007	<b>0.008</b>	0.019
$S = 3$		0.019	<b>0.024</b>

<sup>a</sup>Bold values on the diagonal shown are the  $E$  values from orbitals optimized for that spin state.

$E$  splitting values than those from the state-optimized calculations in Table 9. This resembles the effect of orbital averaging

**Table 9.  $E$  Values ( $\text{cm}^{-1}$ ) Obtained with the Inclusion of Different Spin Multiplicities in the State-Averaging Process<sup>a</sup>**

spin state	[0,1,2,3]	[0,1,2]	[1,2,3]	[2,3]
$S = 1$	0.003	0.003	0.006	
$S = 2$	0.002	0.001	0.002	0.006
$S = 3$	0.003		0.004	0.020

<sup>a</sup>All calculations refer to SA-CASSCF(6,10). Given in square brackets are the spin states included.

for the  $D$  splitting results shown earlier. An observation of note is that the  $S = 2$   $E$  splitting in Table 8, when compared with its partner  $D$ , points to substantial rhombicity ( $E/D = 0.3$ ). The EPR experiments do not indicate any rhombicity. The calculated magnitude of  $E$  reported here is small enough to be around the margin of error for electronic calculations and thus may be too small to draw general conclusions.

## CONCLUSIONS

The challenges to the calculation of electronic structure posed by Kremer's dimer make the molecule an excellent test case for some of the current standard DFT techniques. The simple CASSCF techniques we have employed here are able to treat correctly the various spin states but fall short of quantitative accuracy, as would be expected in the absence of more extensive treatment of the dynamic electron correlation. However, the CASSCF picture appears consistent and provides useful insights into the nature of the ZFS and so may be used to aid the rational design of magnetic materials. Reasonable agreement with experimental results for  $D$  values can be obtained with a state averaged set of orbitals; however the best results are obtained with state-optimized orbitals. The spin–spin coupling is shown to be necessary in gaining good  $D$  values, and its inclusion in calculations for d metals should be encouraged.  $E$  values were calculated to be close to zero, in line with the experimental analysis based on  $C_{3h}$  symmetry. The large number of spin centers in real SMMs may lead to similar problems for standard DFT approaches, and much more exploration into this field is required. CASSCF will not be applicable to larger molecules due to its computational cost. However, the restricted active space (RASSCF) or other multiconfigurational techniques may well be tractable and will indeed be necessary for computational methods to play their role in the design of magnetic nanomaterials.

## AUTHOR INFORMATION

### Corresponding Author

\*E-mail: simonbennie@student.manchester.ac.uk

### Author Contributions

The manuscript was written through contributions of all authors. All authors have given approval to the final version of the manuscript.

### Funding

This work was supported by the Engineering and Physical Sciences Research Council (EPSRC UK).

### Notes

The authors declare no competing financial interest.

## REFERENCES

- (1) Gatteschi, D.; Sessoli, R.; Cornia, A. *Chem. Commun.* **2000**, 25, 725–732.
- (2) Bogani, L.; Wernsdorfer, W. *Nat. Mater.* **2008**, 7, 179–188.
- (3) Cirera, J.; Ruiz, E.; Alvarez, S.; Neese, F.; Kortus, J. *Chem.—Eur. J.* **2009**, 15, 4078–4087.
- (4) Neese, F.; Pantazis, D. A. *Faraday Discuss.* **2011**, 148, 229–238.
- (5) Schmitt, S.; Jost, P.; Van Wuellen, C. *J. Chem. Phys.* **2011**, 134, 194113.
- (6) Neese, F. *J. Am. Chem. Soc.* **2006**, 128, 10213–10222.
- (7) Kaupp, M.; Bühl, M.; Malkin, G. *Calculation of NMR and EPR Parameters: Theory and Applications*; Wiley: Weinheim, Germany, 2004; pp 540–564.
- (8) Hess, B.; Marian, C.; Wahlgren, U.; Gropen, O. *Chem. Phys. Lett.* **1996**, 251, 365–371.
- (9) Neese, F. *J. Chem. Phys.* **2005**, 122, 034107.
- (10) Neese, F. *J. Chem. Phys.* **2007**, 127, 164112.
- (11) Ganyushin, D.; Neese, F. *J. Chem. Phys.* **2006**, 125, 024103.
- (12) Bennie, S. J.; Collison, D.; McDouall, J. J. W. *Dalton* **2012**, submitted.
- (13) Bolster, D. E.; Gutlich, P.; Hatfield, W. E.; Kremer, S.; Muller, E. W.; Wieghardt, K. *Inorg. Chem.* **1982**, 22, 1725–1729.
- (14) Kremer, S. *Inorg. Chem. Soc.* **1985**, 24, 887–890.

- (15) Frisch, M. J.; Trucks, G. W.; Schlegel, H. B.; Scuseria, G. E.; Robb, M. A.; Cheeseman, J. R.; Scalmani, G.; Barone, V.; Mennucci, B.; Petersson, G. A.; Nakatsuji, H.; Caricato, M.; Li, X.; Hratchian, H. P.; Izmaylov, A. F.; Bloino, J.; Zheng, G.; Sonnenberg, J. L.; Hada, M.; Ehara, M.; Toyota, K.; Fukuda, R.; Hasegawa, J.; Ishida, M.; Nakajima, T.; Honda, Y.; Kitao, O.; Nakai, H.; Vreven, T.; Montgomery, J. A., Jr.; Peralta, J. E.; Ogliaro, F.; Bearpark, M.; Heyd, J. J.; Brothers, E.; Kudin, K. N.; Staroverov, V. N.; Kobayashi, R.; Normand, J.; Raghavachari, K.; Rendell, A.; Burant, J. C.; Iyengar, S. S.; Tomasi, J.; Cossi, M.; Rega, N.; Millam, J. M.; Klene, M.; Knox, J. E.; Cross, J. B.; Bakken, V.; Adamo, C.; Jaramillo, J.; Gomperts, R.; Stratmann, R. E.; Yazyev, O.; Austin, A. J.; Cammi, R.; Pomelli, C.; Ochterski, J. W.; Martin, R. L.; Morokuma, K.; Zakrzewski, V. G.; Voth, G. A.; Salvador, P.; Dannenberg, J. J.; Dapprich, S.; Daniels, A. D.; Farkas, O.; Foresman, J. B.; Ortiz, J. V.; Cioslowski, J.; Fox, D. J. *Gaussian 09*, revision B.01; Gaussian, Inc.: Wallingford, CT, 2010.
- (16) Neese, F. An Ab Initio, DFT and Semiempirical SCF MO Package. [Http://www.thch.uni-Bonn.de/dc/orca/](http://www.thch.uni-Bonn.de/dc/orca/) (accessed October 2012)
- (17) Perdew, J. P.; Burke, K.; Ernzerhof, M. *Phys. Rev. Lett.* **1996**, *77*, 3865–3868.
- (18) Tao, J. M.; Perdew, J. P.; Staroverov, V. N.; Scuseria, G. E. *Phys. Rev. Lett.* **2003**, *91*, 146401.
- (19) Lee, C.; Yang, W.; Parr, R. *Phys. Rev. B.* **1988**, *37*, 785–789.
- (20) Becke, A. D. *Phys. Rev. A.* **1988**, *38*, 3098–3100.
- (21) Becke, A. D. *J. Chem. Phys.* **1993**, *98*, 1372–1377.
- (22) Becke, A. D. *J. Chem. Phys.* **1993**, *98*, 5648–5652.
- (23) Zhao, Y.; Truhlar, D. G. *Theor. Chem. Acc.* **2008**, *120*, 215–41.
- (24) Zhao, Y.; Truhlar, D. G. *J. Chem. Phys.* **2006**, *125* (194101), 1–1.
- (25) Chang, C.; Pélassier, M.; Durand, P. *Phys. Scr.* **1986**, *34*, 394.
- (26) Heully, J. L.; Lindgren, I.; Lindroth, E.; Lundqvist, S.; Mårtensson-Pendrill, A. *M. J. Phys. (Paris)* **1986**, *19*, 2799.
- (27) Van Lenthe, E.; Baerends, E. J.; Snijders, J. G. *J. Chem. Phys.* **1993**, *99*, 4597.
- (28) Hess, B. *Phys. Rev. A* **1986**, *33*, 3742–3748.
- (29) Weigend, F.; Ahlrichs, R. *Phys. Chem. Chem. Phys.* **2005**, *7*, 3297–3305.
- (30) Weigend, F.; Furche, F.; Ahlrichs, R. *J. Chem. Phys.* **2003**, *119*, 12753–12762.
- (31) Wieghardt, K.; Chaudhuri, P.; Nuber, B.; Weiss, J. *Inorg. Chem.* **1982**, *21*, 3086–3090.